Toxicon:X 26 (2025) 100220

Contents lists available at ScienceDirect

Toxicon: X

journal homepage: www.journals.elsevier.com/toxicon-x

Oligomer assembly of *Bacillus thuringiensis* Cyt2Aa2 on lipid membranes reveals a thread-like structure

Chontida Tangsongcharoen [a], Jose L. Toca-Herrera [b], Boonhiang Promdonkoy [c], Kanokporn Srisucharitpanit [a], Sudarat Tharad [d,*]

[a] Faculty of Allied Health Sciences, Burapha University, Chonburi, 20131, Thailand
[b] Institut für Biophysik, Department für Bionanowissenschaften, Universität für Bodenkultur Wien (BOKU), Vienna, 1190, Austria
[c] National Center for Genetic Engineering and Biotechnology, National Science and Technology, Development Agency, Pathumthani, 12120, Thailand
[d] Department of Biology, Faculty of Science, Burapha University, Chonburi, 20131, Thailand

ARTICLE INFO

Handling Editor: Dr. Denise Tambourgi

Keywords:
Bacillus thuringiensis
Cytolytic protein
Cyt2Aa2 protein
Oligomer assembly
Fusilli-like structure
Thread-like filament structure

ABSTRACT

Bacillus thuringiensis, a well-known insecticidal bacterium, produces several insecticidal proteins, including cytolytic (Cyt) proteins. Cyt proteins bind directly to the lipid membrane and form large protein complexes. In addition to the protein ladder bands, information on the oligomeric structure in lipid membranes is necessary to understand the mechanism of Cyt proteins on target cells. In this work, we have investigated the oligomeric Cyt2Aa2 complex with synthetic lipid and with erythrocyte membranes. When the activated Cyt2Aa2 protein was incubated with these lipid membranes, the protein ladder pattern relevant to hemolytic activity was detected in SDS-PAGE. Moreover, AFM topographic images revealed a fusilli-like structure and a ring-like structure for synthetic POPC and POPC/Chol, respectively. Furthermore, TEM micrographs provided an additional information on the oligomeric structure of Cyt2Aa2 in erythrocytes. Cyt2Aa2 appears to oligomerise/aggregate into mixed structures between the filamentous structure and small protein complexes in erythrocytes. In addition, a nanopore was found to be a substructure of the filamentous structure. These results strengthen the understanding of Cyt2Aa2 behavior in these two membrane systems, the fusilli and ring-like structures, depending on the type of lipid membrane. Furthermore, the structure of Cyt2Aa2 in insect target membranes remains to be investigated.

1. Introduction

Bacillus thuringiensis (*Bt*) is a widely known insecticidal bacterium. It produces some of insecticidal proteins during vegetative and sporulation phases (Schnepf et al., 1998). A parasporal crystal composing of crystal (Cry) and cytolytic (Cyt) proteins is produced during the sporulation phase (Hofte and Whiteley, 1989). A vegetative insecticidal protein (Vip) (Estruch et al., 1996) and a secreted insecticidal protein (Sip) (Donovan et al., 2006) are expressed during the vegetative phase. Although the insecticidal proteins share a (insect) larvicidal activity, their amino acid sequences and toxic mechanism are different (Li et al., 1991, 1996). Among *Bt* protein, Cry proteins are extensively used as a bioinsecticide for an insect pest control (Marroquin et al., 2000; Schnepf et al., 1998). In addition, a resistance against this protein emerged such as lepidopterans (Pigott and Ellar, 2007). Thus, a new *Bt* protein candidate has been sought for pesticidal proteins (Khorramnejad et al., 2020). Cyt proteins are one of the potential insecticidal protein candidates. Unlike Cry proteins, Cyt proteins have an alternative action against insects by binding directly to lipid membranes (Gill et al., 1992; Thomas and Ellar, 1983a). Thus, Cyt proteins can be used either alone or in combination with Cry proteins in the insect control strategy.

Cyt proteins are named as Cyt1, Cyt2, and Cyt3 based on a similarity of their amino acid sequences (Crickmore et al., 1995). Prior to exerting cytolytic activity, an inactive protoxin is proteolytically activated (Al-yahyaee and Ellar, 1995) and then Cyt proteins exhibit cytolytic activity against various cell types (Thomas and Ellar, 1983b). Cyt

Abbreviations: Cyt2Aa2 toxin, cytolytic toxin from *Bacillus thuringiensis* subsp. *darmstadiensis*; TEM, transmission electron microscopy; AFM, atomic force microscopy; POPC, 1-palmitoyl,2-oleoyl-sn-glycero-3-phosphocholine; DPPC, 1,2-dipalmitoyl-sn-glycero-3-phosphocholine; Chol, Cholesterol; MLVs, Multilamellar lipid vesicles.

* Corresponding author.
E-mail addresses: chontida.ta@go.buu.ac.th (C. Tangsongcharoen), jose.toca-herrera@boku.ac.at (J.L. Toca-Herrera), boonhiang@biotec.or.th (B. Promdonkoy), kanokporns@go.buu.ac.th (K. Srisucharitpanit), sudarat.td@go.buu.ac.th (S. Tharad).

https://doi.org/10.1016/j.toxcx.2025.100220
Received 21 December 2023; Received in revised form 20 October 2024; Accepted 4 March 2025
Available online 7 March 2025

proteins contain a large hydrophobic region to facilitate interaction with membrane lipids such as phosphatidylchloline, sphingomyelin and cholesterol (Thomas and Ellar, 1983b; Gill et al., 1987; Promdonkoy and Ellar, 2003). Two mechanism models have been used to explain the change of the lipid layer structure due to interaction with Cyt proteins: the formation of pores due to Cyt oligomerisation (Du et al., 1999; Li et al., 1996, 2001; Promdonkoy and Ellar, 2005) and the detergent-type model in which Cyt aggregates on lipid membranes until it reaches an adequate number of molecules to remove the lipid from the membranes (Butko, 2003; Manceva et al., 2005). In this work, the assembly of Cyt2Aa2 oligomers (from *B. thuringiensis* subsp. *darmstadiensis*) into synthetic membrane modeling erythrocytes was demonstrated by AFM topographic imaging and the oligomeric structure in erythrocytes by TEM micrographs. These results improve the understanding of the Cyt2Aa2 oligomerisation process as well as its mechanism.

2. Methods

2.1. Preparation of Cyt2Aa2 protein

Protein production of Cyt2Aa2 was carried out as previously described (Promdonkoy et al., 2004). Briefly, *E. coli* JM109 carrying the pGEM-T-*cyt2Aa2* plasmid was cultured in Luria-Bertani (LB) medium containing 100 μg/ml ampicillin, and the Cyt2Aa2 protein was expressed under the *lac* promoter by induction with 1 mM IPTG (Isopropyl β-D-1-thiogalactopyranoside) (ThermoScientific, USA). The Cyt2Aa2 inclusion protein was then solubilized in 50 mM carbonate buffer, pH 10.0 at 30 °C for 1 h. The soluble Cyt2Aa2 was separated from the debris by centrifugation at 10,000g for 10 min. For proteolytic activation, the protein was digested with 2% (w/w) chymotrypsin (Sigma, Germany) at 30 °C for 2 h. Prior use, protein purity and molecular weight of Cyt2Aa2 were evaluated by SDS-PAGE. Protein concentration was determined by UV280 absorption.

2.2. Preparation of lipid vesicles

The lipids used for vesicle formation were 1-palmitoyl,2-oleoyl-snglycero-3-phosphocholine (POPC), 1,2-dipalmitoyl-sn-glycero-3-phosphocholine (DPPC) and cholesterol (Sigma, Germany). The lipids were mixed in chloroform with desired compositions, pure POPC, POPC/Chol (1:1 mol ratio), and POPC/DPPC (1:1 mol ratio). The chloroform was removed by gentle nitrogen stream and kept under the nitrogen stream for at least 1 h to form the lipid film and remove the residual solvent. The lipid film was rehydrated with phosphate buffered saline (PBS), pH 7.4 (Sigma, Germany) at the temperature higher than T_m (POPC at 25 °C and DPPC at 50 °C) for 1 h and then vortexed until complete resuspension to form the multilamellar lipid vesicles with a final concentration of 1 mg/ml. To form unilamellar lipid vesicles for lipid bilayer preparation, the suspended lipid film was homogenized by extruding through a 50 nm polycarbonate membrane using a Mini-Extruder (Avanti, USA). After vesicle preparation, the lipid vesicles were used on the same day or kept at temperatures higher than Tm not more than a week.

2.3. Protein complex formation of Cyt2Aa2 with lipid vesicles

The 100 μg of multilamellar lipid vesicles were incubated with 5 μg of activated Cyt2Aa2 at 25 °C for 2 h. The membrane-bound protein was then separated by centrifugation at 15,000g, 4 °C for 30 min. The protein ladder (protein size) of Cyt2Aa2 was determined by SDS-PAGE, the pellet was resuspended in protein sample loading buffer (without heating the sample) and applied to a NuPAGE Bis-Tris 4–12% gradient gel (Invitrogen, USA). Protein bands were visualized using SimplyBlue SafeStain (Invitrogen, USA).

2.4. Immunodetection of Cyt2Aa2 complexes on erythrocytes

Erythrocytes of sheep blood (Oxoid, ThermoScientific, USA) were isolated from blood serum by centrifugation at 3,000g, 4 °C for 5 min. The erythrocytes were washed three times with PBS, pH 7.4. The erythrocyte pellet was resuspended in PBS, pH 7.4 to 2% (v/v) as a working solution. The 400 μl of prepared erythrocytes were incubated with 400 μl of activated Cyt2Aa2 at different protein concentrations at 25 °C for 2 h. The membrane-bound complex was collected by centrifugation at 15,000g, 4 °C for 30 min. The protein complex was separated by SDS-PAGE (without heating the sample) and detected by a specific antibody against the Cyt2Aa2 protein. The Cyt2Aa2 complex was separated by using 12% polyacrylamide gel and transferred onto nitrocellulose membrane (Whatman, Merck, Germany) by wet-blotting technique. Non-specific protein binding was prevented by 5% (w/v) skim milk (Difco, BD Biosciences, USA) in PBS, pH 7.4 at 4 °C for at least 2 h. Then, the membrane was incubated with a rabbit polyclonal anti-Cyt2Aa2 antibody (1: 8000) (a rabbit polyclonal antibody against Cyt2Aa2 was produced by Center for Agricultural Biotechnology, Kasetsart University, Thailand) at ambient temperature for 2 h and washed with PBST (PBS, pH 7.4 containing 0.1% (v/v) Tween 20) for 5 min, three times. The membrane was then incubated with goat anti-rabbit IgG conjugated horseradish peroxidase (1: 10,000) (Kirkegaard & Perry Laboratories, USA) at ambient temperature, and washed with PBST for 5 min, three times. Finally, Cyt2Aa2 protein was detected by adding enhanced chemiluminescent (ECL) substrate (ThermoScientific pierce, USA) for 5 min and exposed to film.

2.5. Atomic force microscopy (AFM) imaging of Cyt2Aa2-lipid layers

The topography of the Cyt2Aa2-lipid structures was visualized by AFM technique. Silicon-nitride AFM cantilevers with a nominal spring constant of 0.24 N/m (DNP-S10, Bruker, USA) and 1 × 1 cm silicon wafers (IMEC, Leuven, Belgium) were mounted inside a closed fluid cell with an O-ring. The Cyt2Aa2-lipid membrane interaction was visualized on the silicon wafers. The cleaning of the silicon wafers was carried out in four steps: (i) sonication in 2% (w/v) SDS for 20 min, (ii) rinsing with ultrapure water, (iii) drying under nitrogen stream, and (iv) treatment with plasma cleaner for 30 min (Diener electronic, Germany). The AFM cantilevers were also cleaned by plasma cleaner for 30 min. The chamber (fluid cell) was rinsed with PBS, pH 7.4 by using syringe injection and the system was left until the deflection signal was stable. The lipid bilayers were formed by means of lipid vesicle fusion. The 0.1 mg/ml of lipid vesicle solutions were incubated over the silicon surface for at least 10 min and then the vesicle excess was rinsed from the chamber. Afterwards, 25 μg/ml activated Cyt2Aa2 solution was incubated with the lipid bilayers for 2 h. The experiments were throughly conducted at 25 °C. The AFM images were obtained in tapping mode with a JV-scanner controlled by NanoScope V controller (Bruker, USA) at a scan rate of 1–2 Hz. All the images were processed and analyzed using the Nanoscope analysis program.

2.6. Transmission electron microscopy (TEM) of Cyt2Aa2 complex with erythrocytes

Erythrocytes were prepared as described in section 2.4. The 200 μl of 2% (v/v) erythrocytes were incubated with 200 μl of 25 μg/ml activated Cyt2Aa2 solution at 25 °C for 2 h. As a negative control, MilliQ water was used to lyse erythrocytes. The membrane-bound complex was collected by centrifugation at 15,000g, 4 °C for 30 min. The protein complex was washed with 400 μl of PBS, pH 7.4 and collected by centrifugation. Finally, the protein complex was resuspended with 50 μl of PBS, pH 7.4 or 0.1% (v/v) Triton X-100 in PBS. For sample negative staining, 3.05 mm copper grids (Athene Old 300) (Athene, UK) were placed on the sample solution for 1 min followed by 1% (v/v) uranyl acetate for 5 min. The TEM micrographs were taken at 180 kV using a

FEI Tecnai G^2 (Field Electron and Ion Company, USA).

3. Results

3.1. Cyt2Aa2 assembly on lipid vesicles as a protein ladder pattern

Multilamellar lipid vesicles (MLVs) were incubated with activated Cyt2Aa2 at 25 °C for 2 h and the ladder pattern was subsequently determined by SDS-PAGE. Fig. 1 shows that Cyt2Aa2 sedimented with the MLVs after centrifugation as revealed by the ladder pattern with POPC and POPC/Chol but not with DPPC. This suggests that Cyt2Aa2 was able to bind and form a protein complex with unsaturated POPC but was unable to bind saturated DPPC. The ladder bands of the Cyt2Aa2 complex should be due to the effect of SDS as it is a protein denaturing agent.

On the one hand, a mild zwitterionic detergent, Triton X-100 was used to extract the Cyt2Aa2 complex from the lipid vesicles comparing to SDS, and the ladder pattern was determined by the perfluorooctanoic acid-polyacrylamide gel electrophoresis (PFO-PAGE). The results showed that SDS dissociated the Cyt2Aa2 complex into the ladder bands, whereas Triton X-100 did not produce the ladder bands, even under heat condition (Fig. S1). As the ladder pattern of the Cyt2Aa2 complex on SDS gel implies the binding of Cyt2Aa2 and lipids, it also raises a number of questions: "how do the Cyt proteins form the protein complex?" and "what is the conformational structure of the protein complex on lipid membranes?". In the following sections, the structure of the Cyt2Aa2 complex on the membranes is shown by AFM and TEM.

The activated Cyt2Aa2 was incubated with the lipid vesicles at 25 °C for 2 h. The membrane-bound protein complex was collected by centrifugation and was subjected to SDS-PAGE. Protein bands were visualized by Coomassie blue staining.

3.2. Relation of Cyt2Aa2 protein ladder and hemolytic activity

In this section, the relationship between the protein complex formation (the ladder bands) and hemolytic activity was determined. Both protoxin and activated Cyt2Aa2 were incubated with the sheep erythrocytes at 25 °C for 2 h. The protein complex was then determined by SDS-PAGE and immunodetection. Fig. 2 shows that Cyt2Aa2 protoxin has two forms either a ~25 kDa monomer or a ~55 kDa dimer. On the gel, the hemoglobin proteins (16 kDa monomer and 32 kDa dimer) (Billett, 1990) were dominant in the protoxin fraction, suggesting that the erythrocytes remain intact. In contrast, the hemoglobin was significantly reduced in the fractions of the activated Cyt2Aa2 (lane 4–7). To determine the protein complex formation, the erythrocyte-Cyt2Aa2 complexes were separated from the unbound protein by centrifugation and were detected with a specific antibody against Cyt2Aa2 protein. For the inactivated Cyt2Aa2 protoxin, as shown in the SDS-gel, the protoxin could not lyse the erythrocytes indicating that the protoxin was unable to bind and form the protein complex with erythrocytes. The protein concentration of activated Cyt2Aa2 was serially diluted from 25 μg/ml to 1.6 μg/ml. In the absence of erythrocytes, activated Cyt2Aa2 showed only the monomeric form on both SDS gel and Western blots. At protein concentrations of 3.2 μg/ml and 1.6 μg/ml (Fig. 2; lane 7 and 8, respectively), erythrocytes could not be completely lysed due to the presence of hemoglobin in these fractions. In addition, a signal intensity of the protein complexes was related to the protein concentration, with the strong signal corresponding to the high protein concentration. The Cyt2Aa2 complex was detected not only in form of the ladder bands, but also as a large complex in the 4% stacking layer of the gel. Although the protein complex was detectable at the two highest concentrations, complete lysis of erythrocytes was not achieved. Therefore, a protein concentration of 25 μg/ml will be used in further experiments to investigate the protein complex.

Sheep erythrocytes were incubated with different concentrations of activated Cyt2Aa2 at 25 °C for 2 h. Protein complex formation was determined by SDS-PAGE (left) and immunodetection (right). M: protein marker; lane 1: Cyt2Aa2 protoxin; lane 2: Activated Cyt2Aa2; lane 3: 25 μg/ml Cyt2Aa2 protoxin with erythrocytes; lane 4–8: two fold serial dilution of activated Cyt2Aa2.

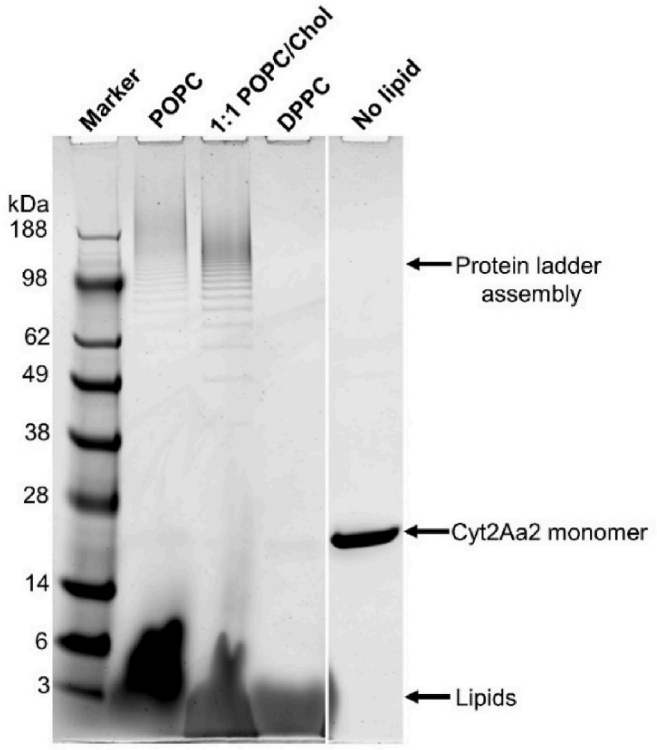

Fig. 1. Protein ladder patterns of Cyt2Aa2 assembly with lipid vesicles.

3.3. Cyt2Aa2 oligomer assembly on the lipid membranes

For the AFM structural studies, two lipid mixtures, 1:1 POPC/DPPC and 1:1 POPC/Chol were considered as the lipid membrane models for erythrocytes. For the 1:1 POPC/DPPC system, the lipid membrane showed a phase separation between POPC (a liquid disordered phase) and DPPC (a solid phase) (Fig. S2). After Cyt2Aa2 exposure, the AFM topographic image revealed that Cyt2Aa2 was unable to bind the saturated DPPC region on the membrane (dark area in Fig. 3A). In contrast, the POPC region was mostly occupied by Cyt2Aa2 protein, which appeared as a fusilli pasta-like structure (Fig. 3B). The results of the AFM images are supported by the formation of ladder bands on POPC but not DPPC membranes (Fig. 1). A specific topographic structure was observed for Cyt2Aa2 aggregation on the lipid membranes; the Cyt2Aa2 complex on the POPC membrane took the form of the fusilli-like structure. The thickness of the fusilli-like complex is approximately 3.0 nm (the difference in height between the Cyt2Aa2-POPC layer and the DPPC area; Fig. 3C). On the contrary, the 1:1 POPC/Chol (a liquid ordered phase) promoted a different structure of the Cyt2Aa2 complex on the membrane. The AFM images showed a ring-like structure (Fig. 4A and B). The diameter of the protein ring structure was approximately 100 nm with a thickness of 1.5 nm (taken from the membrane surface) (Fig. 4C and D).

The lipid membranes were formed by fusing lipid vesicles on the silicon wafer. Then, 25 μg/ml activated Cyt2Aa2 was incubated over the POPC/DPPC lipid surface at 25 °C for 2 h. The surface topography was visualized by AFM tapping mode at a scan rate of 1–2 Hz. (A) The surface topography of Cyt2Aa2-lipid membrane layer. (B) Magnification of (A). (C) Cross-sectional evaluation (height profile) of the Cyt2Aa2 complex as indicated by the white line in (A).

The lipid membranes were formed by fusing lipid vesicles on the

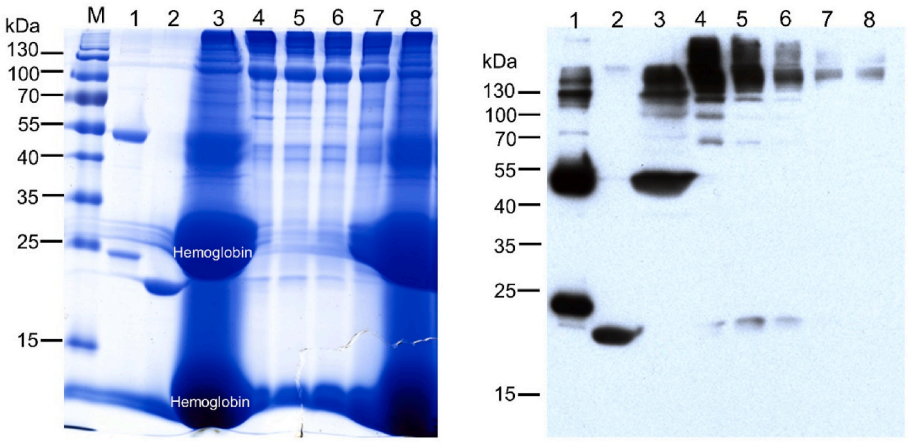

Fig. 2. Cyt2Aa2 complex formation and hemolytic activity relationships.

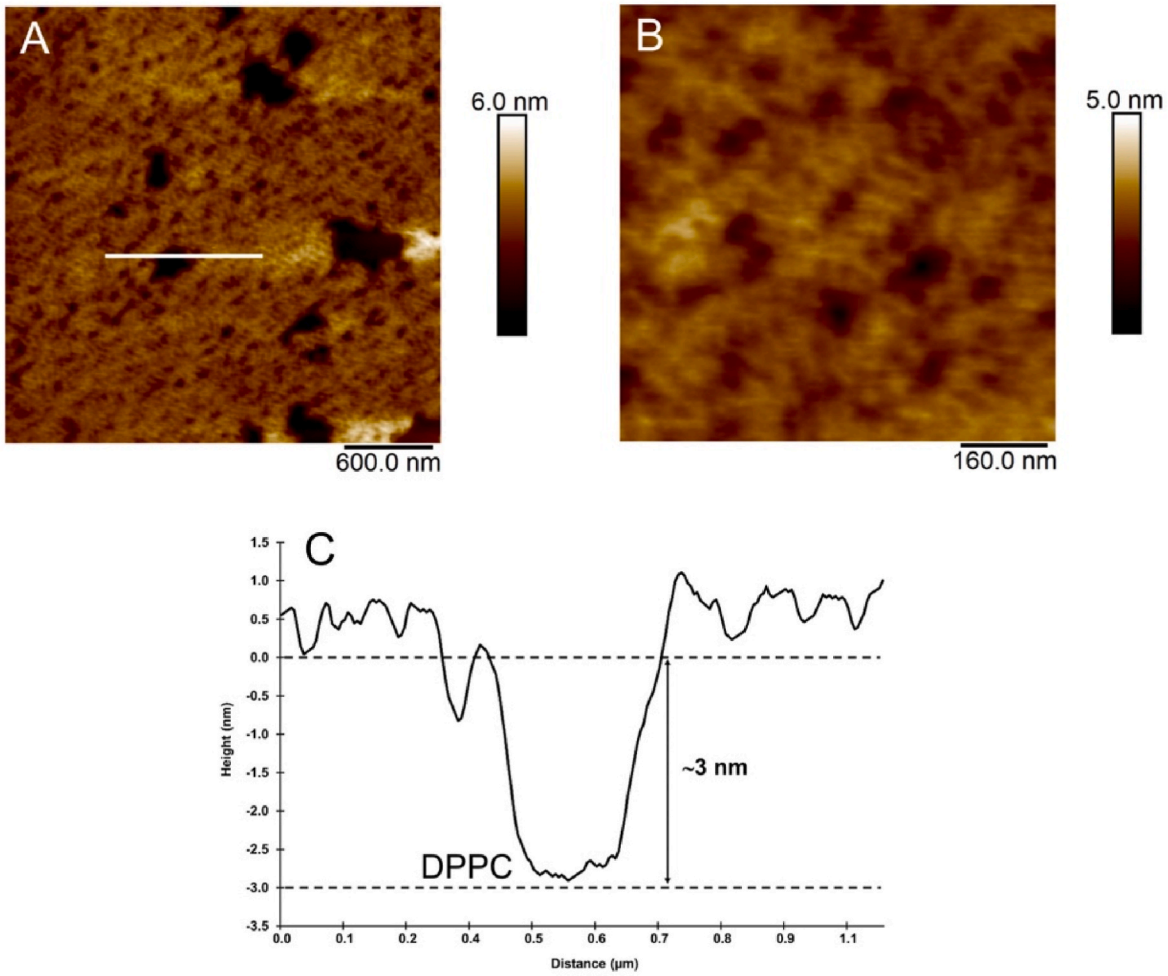

Fig. 3. AFM topographic images of Cyt2Aa2 complex formation on POPC/DPPC membrane.

silicon wafer. Then 25 μg/ml activated Cyt2Aa2 was incubated on the POPC/Chol lipid surface at 25 °C for 2 h. (A) The surface topography of the Cyt2Aa2 complex. (B) Cross-sectional evaluation (height profile) of the Cyt2Aa2 complex as indicated by the white line in (A). The Roman numerals above the height profile indicate the position of the ring structure along the image section in (B). (C) Magnification of (A). (D) cross section of the ring structure in (C). The double-headed arrow indicates a diameter of the ring structure of about 100 nm.

3.4. Structure of Cyt2Aa2 oligomer forming on the erythrocytes

To observe the structure of the Cyt2Aa2 protein complex with cell membranes, Cyt2Aa2 was incubated with erythrocytes at 25 °C for 2 h. The membrane lipids were then removed from the Cyt2Aa2 complex using a mild detergent, Triton X-100. Both forms of the Cyt2Aa2, with and without the erythrocyte membrane, were examined by transmission electron microscopy (TEM). The erythrocytes treated with either

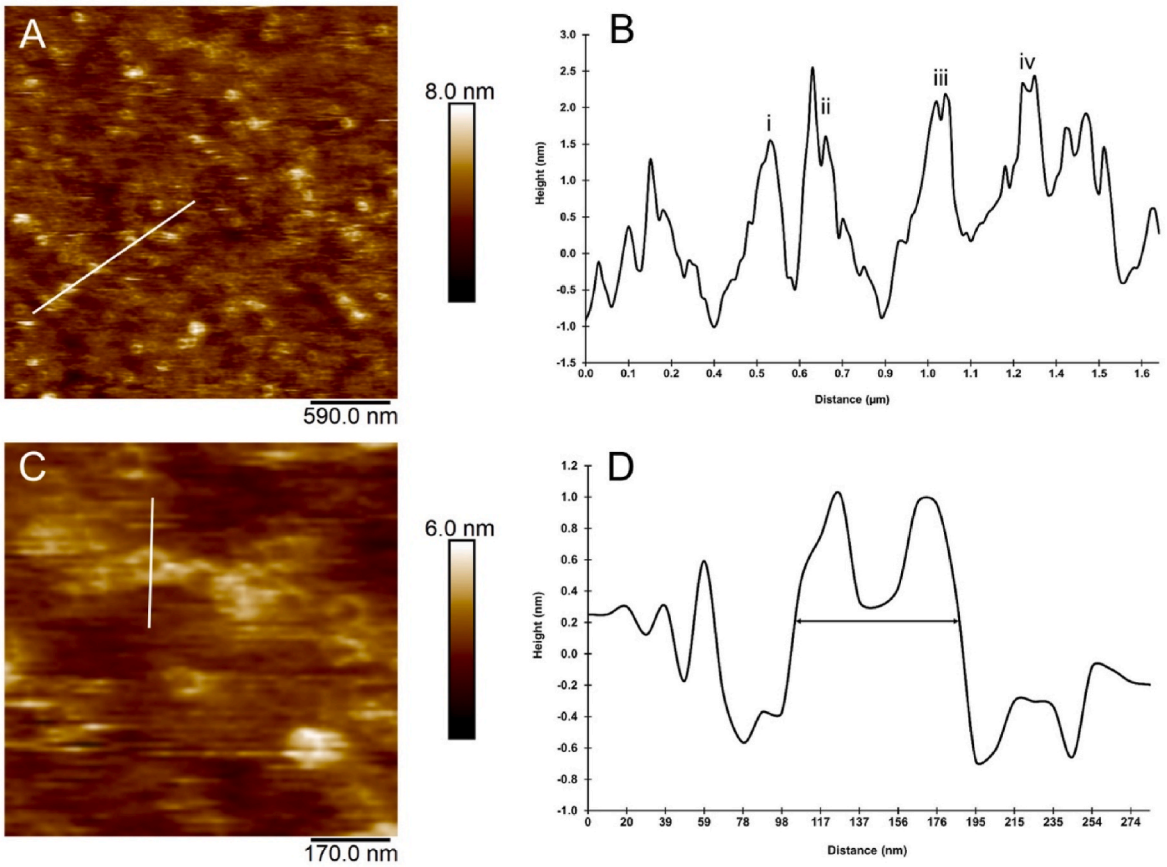

Fig. 4. AFM topographic images of Cyt2Aa2 complex formation on POPC/Chol membrane.

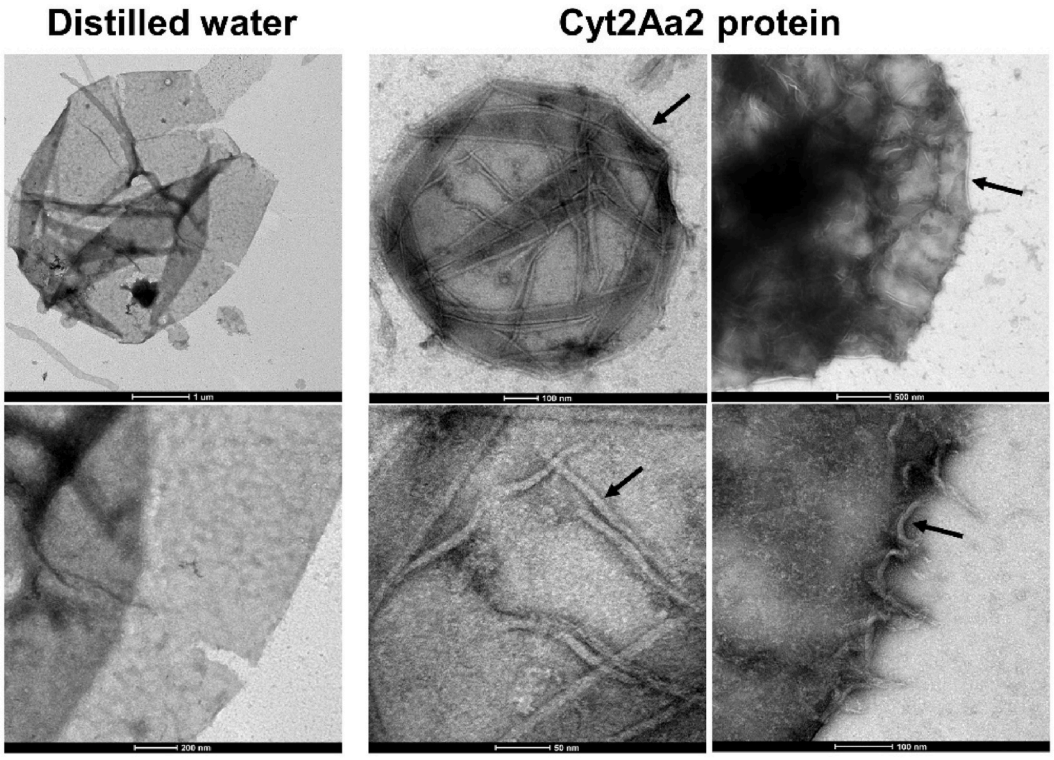

Fig. 5. TEM micrographs of Cyt2Aa2 complex on the erythrocyte membranes.

distilled water (a negative control) or Cyt2Aa2 protein showed different features on the cell membrane (Fig. 5). The water-treated erythrocytes showed a rupture of the lipid membrane (large break in the cell membrane) due to osmotic pressure. On the other hand, the Cyt2Aa2-erythrocyte sample showed a clear layer of Cyt2Aa2 bound to the cell surface of the erythrocytes (indicated by the black arrow), which was absent in the negative control. As shown in the TEM micrographs, the Cyt2Aa2 layer could be observed on the erythrocyte compartment including the folded membranes. In contrast to distilled water, the erythrocyte membrane was ruptured between the membrane-bound Cyt2Aa2 areas. It appears that these areas rupture from the inside due to high pressure. We have proposed that Cyt2Aa2 binds to its target membrane regions, such as POPC or POPC/Chol, and either disrupts membrane integrity or forms pores leading to an osmotic imbalance with high pressure inside the cell.

The erythrocytes were incubated with 25 μg/ml activated Cyt2Aa2 protein at 25 °C for 2 h. The cell membranes were then collected by centrifugation and stained with uranyl acetate for TEM imaging. Black arrows indicate the Cyt2Aa2 layer on the erythrocyte membranes. Distilled water was used as a negative control to lyse the erythrocytes.

As discussed in section 3.1, Triton X-100 greatly reduced the dissociation of the Cyt2Aa2 complex compared to SDS. Thus, the Cyt2Aa2 complex was extracted from the cell membrane by Triton X-100. TEM micrographs showed that the Cyt2Aa2 complex had a filament-like structure (Fig. 6, white arrow). The length of the protein filament complexes varied up to 100 nm with a width of about 20 nm. In contrast to the filament structure, smaller Cyt2Aa2 complexes (Fig. 6, orange arrow) were observed dispersed in the micrograph. Remarkably, a nanopore structure (Fig. 6, blue arrow) appeared within the filamentous protein structure, but was unclear in the smaller complexes. These findings suggest that Cyt2Aa2 protein may form both a linear oligomer (part of the fusilli-like structure) and an arc oligomer (part of the ring structure) depending on the lipid content of the erythrocyte membranes, as shown in the AFM images (Fig. 3).

Cyt2Aa2 complexes were extracted from erythrocytes with 0.1% (v/v) Triton X-100. The protein complexes were rinsed with PBS prior to staining with uranyl acetate. The protein complexes were then collected on a copper grid for TEM imaging. White arrows indicate the filamentous structure and orange arrows indicate the smaller Cyt2Aa2 complexes. A nanopore structure within a filamentous structure is indicated by blue arrows.

4. Discussion

Bacillus thuringiensis, or *Bt*, is a bacterium widely known for its insecticidal properties. The cytolytic protein (Cyt) is a type of *Bt* protein. Over a decade of research has shown that Cyt proteins bind directly to the lipid membrane and form large protein complexes (Gill et al., 1992; Thomas and Ellar, 1983a). Two possible models have been used to explain the actions of Cyt proteins: the pore formation (Du et al., 1999; Li et al., 1996, 2001; Promdonkoy and Ellar, 2005) and the detergent-like model (Butko, 2003; Manceva et al., 2005). However, the explicit mechanism of Cyt proteins has required experimental data to support it. In recent years, the structure of the Cyt complex has been elucidated, providing more information about its molecular mechanism. Therefore, we used AFM and TEM to investigate the surface topography and structure of Cyt2Aa2 complexes on the erythrocyte membrane system.

To determine the lipid membrane binding of Cyt protein family, the protein ladder bands on SDS-PAGE are their fingerprint. In addition, the protein ladder bands related to Cyt2Aa2 activity such the lipid vesicle leakage (Tharad et al., 2016). The Cyt2Aa2 protein showed the ladder pattern with POPC and 1:1 POPC/Chol MLVs but not with DPPC (Fig. 1). In addition, the ladder pattern was shown resulting from dissociation of the large Cyt2Aa2 complex by SDS (Fig. S1). Not only the Cyt2Aa2 protein, but also the ladder banding pattern has been observed for a cardiotoxic volvatoxin A2 (the Cyt-like toxin) (Weng et al., 2004) and the filamentous β2-microglobulin (when dissociated by the reducing agent dithiothreitol (DTT)) (Liu et al., 2011) as well. The results indicated that the ladder pattern was indicative of Cyt2Aa2 complex

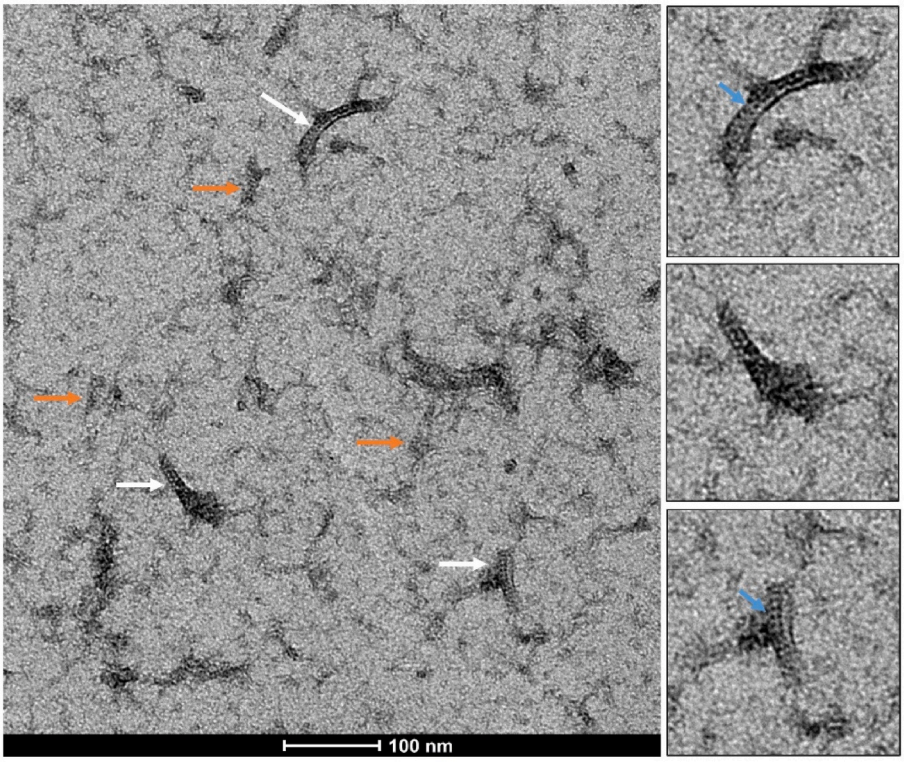

Fig. 6. TEM micrographs of Cyt2Aa2 complex extracted from the erythrocytes.

formation with lipid membranes.

Cyt2Aa2 shows cytolytic activity against various cell types including erythrocytes, where it shows a hemolytic activity. Therefore, the protein ladder bands of Cyt2Aa2 protein were also determined on erythrocytes. The SDS gel results indicated that inactivated Cyt2Aa2 protoxin could not lyse erythrocytes, suggesting that the protoxin was unable to bind and form a protein complex with them. The presence of high molecular weight aggregates of protoxin with erythrocytes suggests that these forms were likely sedimented during centrifugation due to their molecular weight.

Consistent with this, the protoxin also exhibited high molecular weight aggregation in the absence of erythrocytes, whereas the activated Cyt2Aa2 appeared only in its monomeric form on both SDS-gel and Western blot. Subsequently, the formation of protein complexes of the activated Cyt2Aa2 protein was observed on the erythrocytes. Similarly, the protein ladder pattern was detected when Cyt2Aa2 protein was incubated with the erythrocytes, as seen in the MLVs. Moreover, the ladder pattern was relevant to hemolytic activity (Fig. 2), suggesting that the ladder pattern observed on the SDS-PAGE was necessary for Cyt2Aa2 activity. Accordingly, Cyt1Aa forming the membrane-bound oligomers (MBO) shows cytotoxicity against insect Sf21 cells, mammalian NIH fibroblast and HEK293 cells (Tetreau et al., 2020). Molecular weight calculations suggest that the Cyt2Aa2 complexes appearing in stacking gel might be composed of more than 10 monomers (~250 kDa). The hemolytic activity test also indicated that at low concentrations of Cyt2Aa2 (3.2 μg/ml and 1.6 μg/ml), most of erythrocytes remained intact. These results suggest that Cyt2Aa2 monomer should accumulate on the cell membrane and form the protein complex to exert its action. This finding agrees with the previous study on lipid vesicles, where Cyt2Aa2 bound to the lipid membrane without membrane disruption until a critical protein/lipid ratio was reached (Tharad et al., 2016). However, the ladder pattern could not determine the structure of Cyt2Aa2 complexes on POPC, POPC:Chol, and erythrocyte membranes. Besides the protein ladder bands, information of the oligomeric structure on the lipid membranes is necessary to understand the mechanism of Cyt proteins on target cells.

The oligomeric structure of the Cyt2Aa2 protein was then determined using AFM. Two lipid membrane models of erythrocytes were used: (i) 1:1 POPC/DPPC, which exhibits phase separation of liquid disordered and solid phases, at 25 °C (Fig. S2), and (ii) 1:1 POPC/Chol, which forms a liquid ordered phase (Himbert et al., 2017). These findings revealed the different binding of Cyt2Aa2. Cyt2Aa2 bound to the POPC membrane in a fusilli-like structure but could not bind to the DPPC membrane (Fig. 3). For the 1:1 POPC/Chol membrane, AFM images showed a ring-like structure (Fig. 4A and B). Thus, the composition of the lipid membrane influences the Cyt2Aa2 complex structure.

The AFM images confirmed the lipid binding of Cyt2Aa2 protein on MLVs (Fig. 1). Furthermore, AFM images revealed that although the protein complex structure on POPC and POPC/Chol membranes differed, they exhibited similar ladder bands on SDS-gel. The fusilli-like structure was observed in the POPC area with thickness of about 3 nm. These findings suggest that Cyt2Aa2 does not insert into the lipid membrane, as the thickness of the protein complex and the size of the Cyt2Aa2 molecule are similar (Li et al., 1996). In contrast, the 1:1 POPC/Chol mixture promoted a different structure of Cyt2Aa2 complex on the membrane. AFM images revealed the ring-like structure with a diameter of 100 nm and a thickness of 1.5 nm, suggesting that Cyt2Aa2 could insert into the membrane to form this ring structure. The erythrocyte cell membrane has a fluid membrane (liquid disordered phase) and lipid rafts (liquid ordered phase) (Vahedi et al., 2020), indicating that both types of Cyt2Aa2 complex structure could coexist in the erythrocyte membrane. Similarly, properties of lipid membranes had an impact on the Cyt1Aa mechanism. Cyt1Aa molecule is located on the lipid membrane surface for the lipid vesicles (without protein insertion) (Onofre et al., 2020). This action of Cyt1Aa may resemble that of Cyt2Aa2 acting on the POPC membrane, forming the fusilli-like structure without protein insertion. Conversely, the beta strands and helix of Cyt1Aa insert deeply into the brush border membrane vesicle (BBMV) (Onofre et al., 2020), similar to Cyt2Aa2 insertion that forms the ring structure on the POPC/Chol membrane. This study, using lipid membrane models of erythrocyte membrane, provides a state-of-the-art view of the interaction of Cyt2Aa2 with different synthetic lipid membranes. These findings suggest that Cyt2Aa2 may interact differently on the target cell membranes depending on the lipid composition, consistent with our previous study (Tharad et al., 2019). Additionally, protein concentration also affects the lipid binding behavior of Cyt2Aa2 (Tharad et al., 2015).

Furthermore, TEM micrographs revealed the oligomeric Cyt2Aa2 structure in erythrocytes (Fig. 5). After incubation with Cyt2Aa2, a layer of Cyt2Aa2 was observed on the erythrocyte surface, and membrane rupture occurred between the membrane-Cyt2Aa2 areas. In contrast, no such layer was observed on the erythrocyte surface and the cell membrane was teared due to the osmotic pressure. Based on the TEM micrographs, we propose that Cyt2Aa2 binds to target membrane areas such as POPC or POPC/Chol, either disrupting membrane integrity or forming pores, leading to an osmotic pressure imbalance with high internal pressure. The lipid binding areas of Cyt2Aa2 can create tension in unbound regions of the membrane (such as the saturated lipid region), making them more susceptible to rupture due to osmotic pressure. Conversely, the Cyt2Aa2-lipid layer is more rigid than the Cyt2Aa2-free membrane regions, making it more resistant to breakage. As shown in Fig. 5, the lesion on the erythrocyte membrane can be up to 50 nm in diameter, which is larger than the expected size of Cyt selective channels with 6–20 Å diameter (Drobniewski and Ellar, 1988). The TEM micrograph is consistent with previous findings using insect Sf21 and mammalian NIH 3T3 cells, where Cyt1Aa induced lesions rather than the selective pores, as evidenced by penetration of 8.5 nm fluorescent beads into the cells (Tetreau et al., 2020). Consequently, Cyt2Aa2 oligomeric complexes were isolated from erythrocyte membranes using Triton X-100, which does not dissociate the Cyt2Aa2 complex. The Cyt2Aa2 complex exhibited a filamentous, thread-like structure with varying lengths and a width of about 20 nm (Fig. 6). Interestingly, a nanopore-structure was observed as part of the thread-like protein structure. The filamentous structure was previously reported for both Cyt1A and Cyt2A proteins. The filamentous oligomeric structure of Cyt2Aa with POPC lipid vesicle was experimentally observed by cryo-EM (Šolinc et al., 2023) and the arc filament structure of Cyt1Aa with lipid vesicle (10:3:1 egg yolk phosphatidyl choline: cholesterol: stearylamine) was revealed by cryo-EM and TEM (Tetreau et al., 2020). These findings, along with the previous reports, suggest that the filament thread-like structure of Cyt2Aa2 may be part of either the fusilli-like structure (a linear oligomer) or the ring structure (an arc oligomer) depending on the lipid content in the erythrocyte membranes as shown in the AFM images (Figs. 3 and 4). In addition, smaller Cyt2Aa2 complexes were also observed. These complexes may form on smaller membrane regions of the erythrocytes than where the filament structure occurs, or they may dissociate from the filamentous structure. The nanopore in the filamentous structure is a reasonable size to be the selective channels of Cyt proteins, as previously reported by Drobniewski and Ellar in 1988. Based on the results of this work, Cyt2Aa2 protein can form different structures depending on the membrane type, consistent with our previous report (Tharad et al., 2019). Although the mechanism of Cyt proteins has been investigated for several decades, the precise mechanism remains unclear.

Together with the AFM topography and TEM micrograph, these results enhanced the understanding of the behavior of Cyt2Aa2 binding and forming the oligomeric structure on the membrane. Based on this work, we propose a mechanism for Cyt2Aa2 protein interaction with lipid membranes. For the POPC fluid membrane, Cyt2Aa2 protein may disrupt the lipid membrane through the following steps: (i) binding of active monomeric Cyt2Aa2 protein to lipid membranes, (ii) conformational changes in the protein, (iii) assembly/accumulation of Cyt2Aa2

protein without membrane insertion, (iv) formation of fusilli-like structures, (v) complex structures leading to membrane integrity disruption, and (vi) causing lesions on the membrane (larger than the oligomeric protein pore). Conversely, the membrane with a high cholesterol content (POPC:Chol) may be disturbed by Cyt2Aa2 protein through a slightly different mechanism. The initial steps, the lipid binding and protein conformation change (i and ii), are proposed to be like those in the POPC membrane. The distinct step would occur during protein assembly/accumulation (iii), Cyt2Aa2 protein inserts into the membrane, forming the nanopore and each pore connected to form the filamentous structure, (iv) the filamentous protein grows until it appears as ring shape, (v) the nanopores cause osmotic pressure imbalance and cell bursting as depict in the TEM micrograph (Fig. 5). Combining our data with other studies on Cyt proteins, we find similar results: (i) Cyt proteins show a protein ladder pattern on SDS-PAGE when forming protein complexes, and this pattern is related to their cytolytic activity; (ii) Cyt accumulates on lipid membranes to exert their action. In the pore-forming model, Cyt2Aa2 protein can form pores that connect to be the filamentous structure, which differs from other pore-forming toxins such as alpha hemolysin (Song et al., 1996) or Cytolysin A (Sathyanarayana et al., 2018), which form individual pores on the membrane. However, the precise mechanism of this complex structure in relation to biological activity and specificity on the target membranes/cells is still under investigation and requires more data support, such as measured by Electrochemical Quartz Crystal Microbalance with Dissipation Monitoring (EQCM-D), which can provide the data of protein-lipid interaction simultaneously with membrane leakage. Future work will involve screening lipid membranes that mimic the insect target membranes for the specific structure of Cyt2Aa2 protein.

5. Conclusions

This work describes the oligomeric assembly of Cyt2Aa2 protein with synthetic lipid membranes and erythrocyte membranes. In general, the protein complexes of Cyt2Aa2 with lipid vesicles (except the DPPC) were observed as the ladder bands on SDS-PAGE, correlating with its hemolytic activity. AFM topographic images revealed distinct protein-lipid structures influenced by the lipid content of the membranes: the fusilli-like structure was found with POPC membranes, while the ring-shaped structure was observed with POPC/Chol membranes. Additionally, TEM micrographs showed the oligomeric assembly of Cyt2Aa2 as the thread-like structures. These findings provide a better understanding of the Cyt2Aa2 mechanism and its oligomeric complex structure. However, the specific structure of these toxins in the insect target membrane remains to be investigated.

CRediT authorship contribution statement

Chontida Tangsongcharoen: Writing – original draft, Visualization, Methodology, Investigation, Funding acquisition, Formal analysis. **Jose L. Toca-Herrera:** Writing – review & editing, Validation, Supervision, Resources, Project administration, Investigation, Funding acquisition, Data curation, Conceptualization. **Boonhiang Promdonkoy:** Writing – review & editing, Resources. **Kanokporn Srisucharitpanit:** Writing – original draft, Investigation, Funding acquisition, Formal analysis. **Sudarat Tharad:** Writing – original draft, Visualization, Validation, Project administration, Methodology, Investigation, Funding acquisition, Formal analysis, Data curation, Conceptualization.

Ethical statement

No animals or human subjects were used for experiments related to the results of this manuscript.

Funding

This research (Grant number RGNS 65-130) was supported by Office of the Permanent Secretary, Ministry of Higher Education, Science, Research and Innovation (OPS MHESI), Thailand Science Research and Innovation and Burapha University; Thailand Science Research and Innovation (Grant number FF54/2566); the Austrian Science Fund (FWF) (Grant number P35777-B). Finally, the authors would like to acknowledge the generous support of Burapha University to this project.

Declaration of competing interest

The authors declare that they have no known competing financial interests or personal relationships that could have appeared to influence the work reported in this paper.

Acknowledgements

Authors would like to kindly acknowledge Jacqueline Friedmann (Institut für Biophysik, Department für Bionanowissenschaften, Universität für Bodenkultur Wien (BOKU), Vienna) for technical supporting and TEM imaging.

Appendix A. Supplementary data

Supplementary data to this article can be found online at https://doi.org/10.1016/j.toxcx.2025.100220.

Data availability

No data was used for the research described in the article.

References

Al-yahyaee, S.A.S., Ellar, D.J., 1995. Maximal toxicity of cloned CytA delta-endotoxin from *Bacillus thuringiensis* subsp. *israelensis* requires proteolytic processing from both the N- and C-termini. Microbiology 141, 3141–3148. https://doi.org/10.1099/13500872-141-12-3141.

Billett, H.H., 1990. Hemoglobin and hematocrit. In: Walker, H.K., Hall, W.D., Hurst, J.W. (Eds.), Clinical Methods: the History, Physical, and Laboratory Examinations. Butterworth Publishers, Boston, Boston, pp. 718–719.

Butko, P., 2003. Cytolytic toxin Cyt1A and its mechanism of membrane damage: data and hypotheses. Appl. Environ. Microbiol. 69, 2415–2422. https://doi.org/10.1128/AEM.69.5.2415-2422.2003.

Crickmore, N., Bone, E.J., Williams, J.A., Ellar, D.J., 1995. Contribution of the individual components of the δ-endotoxin crystal to the mosquitocidal activity of *Bacillus thuringiensis* subsp. *israelensis*. FEMS (Fed. Eur. Microbiol. Soc.) Microbiol. Lett. 131, 249–254. https://doi.org/10.1111/j.1574-6968.1995.tb07784.x.

Donovan, W.P., Engleman, J.T., Donovan, J.C., Baum, J.A., Bunkers, G.J., Chi, D.J., Clinton, W.P., English, L., Heck, G.R., Ilagan, O.M., Krasomil-Osterfeld, K.C., Pitkin, J.W., Roberts, J.K., Walters, M.R., 2006. Discovery and characterization of Sip1A: a novel secreted protein from *Bacillus thuringiensis* with activity against coleopteran larvae. Appl. Microbiol. Biotechnol. 72, 713–719. https://doi.org/10.1007/s00253-006-0332-7.

Drobniewski, F.A., Ellar, D.J., 1988. Investigation of the membrane lesion induced in vitro by two mosquitocidal δ-endotoxins of *Bacillus thuringiensis*. Curr. Microbiol. 16, 195–199.

Du, J., Knowles, B.H., Li, J., Ellar, D.J., 1999. Biochemical characterization of *Bacillus thuringiensis* cytolytic toxins in association with a phospholipid bilayer. Biochem. J. 338 (Pt 1), 185–193.

Estruch, J.J., Warren, G.W., Mullins, M.A., Nye, G.J., Craig, J.A., Koziel, M.G., 1996. Vip3A, a novel *Bacillus thuringiensis* vegetative insecticidal protein with a wide spectrum of activities against lepidopteran insects. Proc. Natl. Acad. Sci. USA. 93, 5389–5394. https://doi.org/10.1073/pnas.93.11.5389.

Gill, S.S., Cowles, E.A., Pietrantonio, P.V., 1992. The mode of action of *Bacillus thuringiensis* endotoxins. Annu. Rev. Entomol. 37, 615–636. https://doi.org/10.1146/annurev.en.37.010192.003151.

Gill, S.S., Singh, G.J., Hornung, J.M., 1987. Cell membrane interaction of *Bacillus thuringiensis* subsp. *israelensis* cytolytic toxins. Infect. Immun. 55, 1300–1308. https://doi.org/10.1128/iai.55.5.1300-1308.1987.

Himbert, S., Alsop, R.J., Rose, M., Hertz, L., Dhaliwal, A., Moran-Mirabal, J.M., Verschoor, C.P., Bowdish, D.M.E., Kaestner, L., Wagner, C., Rheinstädter, M.C., 2017. The molecular structure of human red blood cell membranes from highly oriented, solid supported multi-lamellar membranes. Sci. Rep. 7, 39661.

Hofte, H., Whiteley, H.R., 1989. Insecticidal crystal proteins of *Bacillus thuringiensis*. Microbiol. Rev. 53, 242–255. https://doi.org/10.1128/mr.53.2.242-255.1989.

Khorramnejad, A., Gomis-Cebolla, J., Talaei-Hassanlouei, R., Bel, Y., Escriche, B., 2020. Genomics and proteomics analyses revealed novel candidate pesticidal proteins in a Lepidopteran-toxic *Bacillus thuringiensis* strain. Toxins 12, 673. https://doi.org/10.3390/toxins12110673.

Li, J., Derbyshire, D.J., Promdonkoy, B., Ellar, D.J., 2001. Structural implications for the transformation of the *Bacillus thuringiensis* delta-endotoxins from water-soluble to membrane-inserted forms. Biochem. Soc. Trans. 29, 571–577. https://doi.org/10.1042/bst0290571.

Li, J., Koni, P.A., Ellar, D.J., 1996. Structure of the mosquitocidal delta-endotoxin CytB from *Bacillus thuringiensis* sp. *kyushuensis* and implications for membrane pore formation. J. Mol. Biol. 257, 129–152. https://doi.org/10.1006/jmbi.1996.0152.

Li, J.D., Carroll, J., Ellar, D.J., 1991. Crystal structure of insecticidal delta-endotoxin from *Bacillus thuringiensis* at 2.5 Å resolution. Nature 353, 815–821. https://doi.org/10.1038/353815a0.

Liu, C., Sawaya, M.R., Eisenberg, D., 2011. β_2-microglobulin forms three-dimensional domain-swapped amyloid fibrils with disulfide linkages. Nat. Struct. Mol. Biol. 18, 49–55. https://doi.org/10.1038/nsmb.1948.

Manceva, S.D., Pusztai-Carey, M., Russo, P.S., Butko, P., 2005. A detergent-like mechanism of action of the cytolytic toxin Cyt1A from *Bacillus thuringiensis* var. *israelensis*. Biochemistry 44, 589–597. https://doi.org/10.1021/bi048493y.

Marroquin, L.D., Elyassnia, D., Griffitts, J.S., Feitelson, J.S., Aroian, R.V., 2000. *Bacillus thuringiensis* (Bt) toxin susceptibility and isolation of resistance mutants in the nematode *Caenorhabditis elegans*. Genetics 155, 1693–1699. https://doi.org/10.1093/genetics/155.4.1693.

Onofre, J., Pacheco, S., Torres-Quintero, M.C., Gill, S.S., Soberon, M., Bravo, A., 2020. The Cyt1Aa toxin from *Bacillus thuringiensis* inserts into target membranes via different mechanisms in insects, red blood cells, and lipid liposomes. J. Biol. Chem. 295, 9606–9617. https://doi.org/10.1074/jbc.RA120.013869.

Pigott, C.R., Ellar, D.J., 2007. Role of receptors in *Bacillus thuringiensis* crystal toxin activity. Microbiol. Mol. Biol. Rev. 71, 255–281. https://doi.org/10.1128/mmbr.00034-06.

Promdonkoy, B., Ellar, D.J., 2003. Investigation of the pore-forming mechanism of a cytolytic delta-endotoxin from *Bacillus thuringiensis*. Biochem. J. 374, 255–259. https://doi.org/10.1042/bj20030437.

Promdonkoy, B., Ellar, D.J., 2005. Structure-function relationships of a membrane pore forming toxin revealed by reversion mutagenesis. Mol. Membr. Biol. 22, 327–337. https://doi.org/10.1080/09687860500166192.

Promdonkoy, B., Promdonkoy, P., Tanapongpipat, S., Luxananil, P., Chewawiwat, N., Audtho, M., Panyim, S., 2004. Cloning and characterization of a mosquito larvicidal toxin produced during vegetative stage of *Bacillus sphaericus* 2297. Curr. Microbiol. 49, 84–88. https://doi.org/10.1007/s00284-004-4274-y.

Sathyanarayana, P., Maurya, S., Behera, A., Ravichandran, M., Visweswariah, S.S., Ayappa, K.G., Roy, R., 2018. Cholesterol promotes Cytolysin A activity by stabilizing the intermediates during pore formation. Proc. Natl. Acad. Sci. U. S. A. 115, E7323–e7330.

Schnepf, E., Crickmore, N., Van Rie, J., Lereclus, D., Baum, J., Feitelson, J., Zeigler, D.R., Dean, D.H., 1998. *Bacillus thuringiensis* and its pesticidal crystal proteins. Microbiol. Mol. Biol. Rev. 62, 775–806. https://doi.org/10.1128/mmbr.62.3.775-806.1998.

Šolinc, G., Anderluh, G., Podobnik, M., 2023. *Bacillus thuringiensis* toxin Cyt2Aa forms filamentous oligomers when exposed to lipid membranes or detergents. Biochem. Biophys. Res. Commun. 674, 44–52. https://doi.org/10.1016/j.bbrc.2023.06.078.

Song, L., Hobaugh, M.R., Shustak, C., Cheley, S., Bayley, H., Gouaux, J.E., 1996. Structure of staphylococcal alpha-hemolysin, a heptameric transmembrane pore. Science 274, 1859–1866.

Tetreau, G., Banneville, A.-S., Andreeva, E.A., Brewster, A.S., Hunter, M.S., Sierra, R.G., Teulon, J.-M., Young, I.D., Burke, N., Grünewald, T.A., Beaudouin, J., Snigireva, I., Fernandez-Luna, M.T., Burt, A., Park, H.-W., Signor, L., Bafna, J.A., Sadir, R., Fenel, D., Boeri-Erba, E., Bacia, M., Zala, N., Laporte, F., Després, L., Weik, M., Boutet, S., Rosenthal, M., Coquelle, N., Burghammer, M., Cascio, D., Sawaya, M.R., Winterhalter, M., Gratton, E., Gutsche, I., Federici, B., Pellequer, J.-L., Sauter, N.K., Colletier, J.-P., 2020. Serial femtosecond crystallography on in vivo-grown crystals drives elucidation of mosquitocidal Cyt1Aa bioactivation cascade. Nat. Commun. 11, 1153. https://doi.org/10.1038/s41467-020-14894-w.

Tharad, S., Iturri, J., Moreno-Cencerrado, A., Mittendorfer, M., Promdonkoy, B., Krittanai, C., Toca-Herrera, J.L., 2015. Effect of the concentration of cytolytic protein Cyt2Aa2 on the binding mechanism on lipid bilayers studied by QCM-D and AFM. Langmuir 31, 10477–10483. https://doi.org/10.1021/acs.langmuir.5b02849.

Tharad, S., Promdonkoy, B., Toca-Herrera, J.L., 2019. Lipid phase influences the binding of *Bacillus thuringiensis* Cyt2Aa2 toxin on model lipid membranes. Biochem. Biophys. Res. Commun. 511, 409–415. https://doi.org/10.1016/j.bbrc.2019.02.072.

Tharad, S., Toca-Herrera, J.L., Promdonkoy, B., Krittanai, C., 2016. *Bacillus thuringiensis* Cyt2Aa2 toxin disrupts cell membranes by forming large protein aggregates. Biosci. Rep. 36. https://doi.org/10.1042/BSR20160090.

Thomas, W.E., Ellar, D.J., 1983a. *Bacillus thuringiensis* var *israelensis* crystal delta-endotoxin: effects on insect and mammalian cells in vitro and in vivo. J. Cell Sci. 60, 181–197. https://doi.org/10.1242/jcs.60.1.181.

Thomas, W.E., Ellar, D.J., 1983b. Mechanism of action of *Bacillus thuringiensis* var *israelensis* insecticidal delta-endotoxin. FEBS Lett. 154, 362–368. https://doi.org/10.1016/0014-5793(83)80183-5.

Vahedi, A., Bigdelou, P., Farnoud, A.M., 2020. Quantitative analysis of red blood cell membrane phospholipids and modulation of cell-macrophage interactions using cyclodextrins. Sci. Rep. 10, 15111. https://doi.org/10.1038/s41598-020-72176-3.

Weng, Y.P., Lin, Y.P., Hsu, C.I., Lin, J.Y., 2004. Functional domains of a pore-forming cardiotoxic protein, volvatoxin A2. J. Biol. Chem. 279, 6805–6814.